

HOT GAS IN THE WOLF-RAYET NEBULA NGC 3199

J.A. TOALÁ (杜宇君)^{1,2}, A.P. MARSTON³, M.A. GUERRERO⁴, Y.-H. CHU (朱有花)¹, AND R.A. GRUENDL⁵¹Institute of Astronomy and Astrophysics, Academia Sinica (ASIAA), Taipei 10617, Taiwan²Instituto de Radioastronomía y Astrofísica, UNAM Campus Morelia, Apartado postal 3-72, Morelia 58090, Michoacán, Mexico³European Space Agency/STScI, 3700 San Martin Drive, Baltimore, MD 21218, USA⁴Instituto de Astrofísica de Andalucía, IAA-CSIC, Glorieta de la Astronomía s/n, Granada 18008, Spain⁵Department of Astronomy, University of Illinois, 1002 West Green Street, Urbana, IL 61801, USA

ABSTRACT

The Wolf-Rayet (WR) nebula NGC 3199 has been suggested to be a bow shock around its central star WR 18, presumably a runaway star, because optical images of the nebula show a dominating arc of emission south-west of the star. We present the *XMM-Newton* detection of extended X-ray emission from NGC 3199, unveiling the powerful effect of the fast wind from WR 18. The X-ray emission is brighter in the region south-east of the star and analysis of the spectral properties of the X-ray emission reveals abundance variations: i) regions close to the optical arc present nitrogen-rich gas enhanced by the stellar wind from WR 18 and ii) gas at the eastern region exhibits abundances close to those reported for nebular abundances derived from optical studies, signature of an efficient mixing of the nebular material with the stellar wind. The dominant plasma temperature and electron density are estimated to be $T \approx 1.2 \times 10^6$ K and $n_e = 0.3 \text{ cm}^{-3}$ with an X-ray luminosity in the 0.3–3.0 keV energy range of $L_X = 2.6 \times 10^{34} \text{ erg s}^{-1}$. Combined with information derived from *Herschel* and the recent *Gaia* first data release, we conclude that WR 18 is not a runaway star and the formation, chemical variations, and shape of NGC 3199 depend on the initial configuration of the interstellar medium.

Keywords: ISM: bubbles — stars: Wolf-Rayet — X-rays: ISM — X-rays: individual (NGC 3199) — X-rays: individual (WR 18)

1. INTRODUCTION

Throughout their lives, before exploding as supernovae, very massive stars ($M_i \gtrsim 30 M_\odot$) modify the structure and enrich the interstellar medium (ISM) by a combination of different factors: stellar winds, strong ionizing photon fluxes, and proper motions. They represent the main source of feedback that governs the physical structures of the ISM.

After evolving off the main sequence stage, very massive stars enter the red supergiant or luminous blue variable phase exhibiting dense, slow (~ 10 – 100 km s^{-1}), and dust-rich winds that expand into the ISM. This slow wind expels more than half of the initial mass of the star, exposing its hot core and becoming a Wolf-Rayet (WR) star. WR stars present strong winds ($v_\infty \approx 1500 \text{ km s}^{-1}$, $\dot{M} \approx 10^{-5} M_\odot \text{ yr}^{-1}$; e.g., Hamann et al. 2006) that sweep up and compress the previously ejected RSG/LBV material into a shell, whilst the newly developed UV flux ionizes the material, forming the so-called ring nebulae or WR nebulae.

Bubble models suggest that this wind-wind interaction produces an adiabatically-shocked region of gas with temperatures as high as $T = 10^7$ – 10^8 K and electron densities of $n_e \approx 10^{-2} \text{ cm}^{-3}$ that fills the nebular shell in-

terior (Dyson & Williams 1997), known as *hot bubble*¹. These hot bubbles have only been detected by X-ray observatories in the WR nebulae around WR 6 (S 308), WR 7 (NGC 2359), and WR 136 (NGC 6888). The best-quality X-ray observations towards these nebulae have been obtained with *XMM-Newton* and model fits to their X-ray spectra suggest plasma temperatures of $T_X = [1$ – $2] \times 10^6$ K, electron densities $n_e \lesssim 1 \text{ cm}^{-3}$, and X-ray luminosities $L_X = 10^{33}$ – $10^{34} \text{ erg s}^{-1}$ (Chu et al. 2003; Toalá et al. 2012, 2015a, 2016). The low temperatures indicated by the soft diffuse X-ray emission are the result of mixing between the hot bubble and the warm ($T = 10^4$ K) nebular material. Properties of this mixing region strongly depend on the formation of hydrodynamical instabilities and can be augmented if thermal conduction is taken into account (e.g., Toalá & Arthur 2011; Dwarkadas & Rosenberg 2013). Consequently, the X-ray-emitting gas exhibits abundances close to those of the nebular material.

The deepest X-ray observation of a WR nebula is that presented by Toalá et al. (2016) of NGC 6888, the most studied object of this class. These authors reported, for

¹ The post-shock temperature in a hot bubble can be expressed as $k_B T = 3 \mu m_H v_\infty^2 / 16$, where μm_H and k_B are the mean mass per particle and the Boltzmann's constant, respectively.

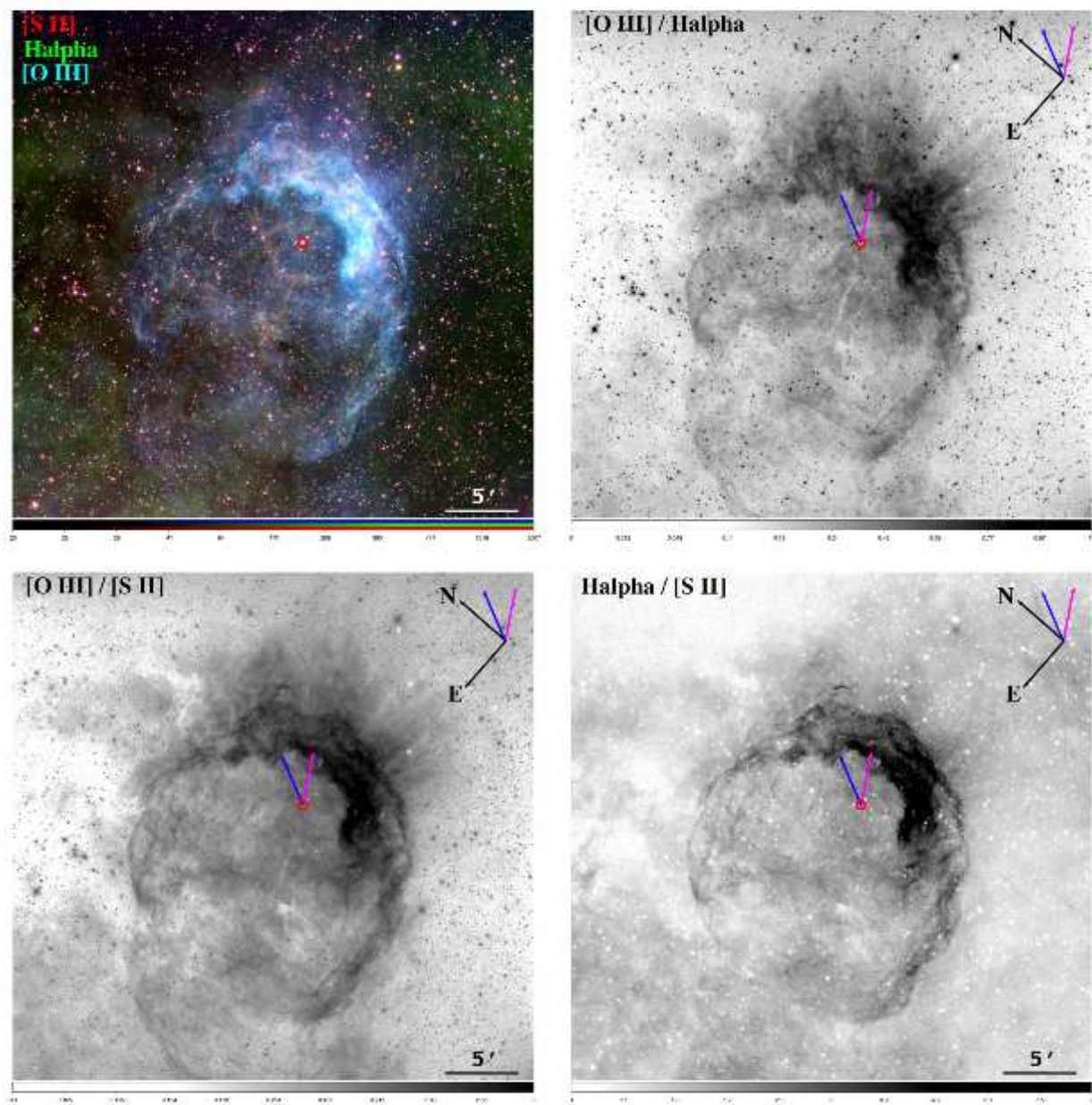


Figure 1. Top left panel: Color-composite nebular image of NGC 3199. The colors red, green, and blue correspond to [S II], H α , and [O III] line emission, respectively. Other panels show the [O III]/H α (top-right), [O III]/[S II] (bottom-left), and H α /[S II] (bottom-right) ratio maps. The position of WR18 is shown with a red circle in all panels and the orientation of the figures is shown on each panel. The blue and magenta arrows show the direction of the proper motions reported by *Hipparcos* and *Gaia* observations, respectively (see text). The narrow-band images are courtesy of Don Goldman.

the first time in the X-ray regime, nitrogen and temperature variations within the WR nebula leading them to the conclusion that the mixing of material is not equally efficient in all directions. Apparently, the mixing has been less efficient towards the caps of NGC 6888, which presents higher temperature and nitrogen abundance, while in the central regions the X-ray-emitting material has similar abundances as those reported for the nebular material (see Reyes-Pérez et al. 2015, and references therein).

On the other hand, there are two other WR nebulae that have not been detected in X-rays. These are RCW 58 around WR 40 and that around WR 16 (Gosset et al. 2005; Toalá & Guerrero 2013). These nebulae harbor WN8h stars with relatively slow stellar winds ($v_\infty \approx 650 \text{ km s}^{-1}$), while those that have been detected in X-rays (S 308, NGC 2359, and NGC 6888) have WN4-6 stars with faster winds ($v_\infty \approx 1700 \text{ km s}^{-1}$; Hamann et al. 2006). Even though this wind velocity seems to be the only characteristic in common for displaying diffuse X-ray emission, it can not be taken with certainty as the current number of studied WR nebulae in the X-ray regime is small and the global properties of the X-ray-emitting gas may depend on other stellar and nebular properties, including the stellar evolution, formation mechanism, ISM structures around the nebulae (see discussion by Toalá et al. 2016).

In this paper, we present *XMM-Newton* observations towards NGC 3199 (see Fig. 1) around the WN4 star WR 18 ($T_{\text{eff}} = 112.2 \text{ kK}$; Hamann et al. 2006). Archival *ROSAT* observations (Obs. ID. RP900318N00) hinted at the presence of diffuse X-ray emission, but the X-ray point sources projected within the nebula, including that of WR 18 (e.g., Skinner et al. 2010), prohibited an unambiguous analysis. Unlike other WR nebulae detected in X-rays, this nebula has been the center of discussions as some authors suggest that the abundances are close to galactic H II regions (see, e.g., Whitehead et al. 1988; Stock et al. 2011), while others suggest that some regions within the nebula exhibit significant chemical enrichment (e.g., Esteban et al. 1992; Marston 2001).

Figure 1 shows in great detail the optical morphology and extension of NGC 3199. The nebula has an elongated shape with angular size of $\sim 20' \times 25'$ as mapped by the [O III] narrow-band emission but with an obvious enhanced emission towards the west, the bright arc (see also Whitehead et al. 1988). This arc was the defining factor for Dyson & Ghanbari (1989) to suggest that NGC 3199 is composed of swept up ISM material in a bow shock around WR 18, which is not located at the geometrical center of the nebula. In fact, *Hipparcos* reported a proper motion for WR 18 of $(\mu_\alpha, \mu_\delta) = (-2.30 \pm 1.75, 4.78 \pm 1.35 \text{ mas yr}^{-1})$ (Perryman et al. 1997), which at a distance of 2.2 kpc (see van der Hucht 2001) corresponds

to a projected velocity of $v_* \approx 55 \pm 20 \text{ km s}^{-1}$ along the north-west direction.

The present paper is organized as follows. The description of our *XMM-Newton* observations and the analysis are presented in Section 2. Our results are presented and discussed in Sections 3 and 4, respectively. We finally summarize our findings in Section 5.

2. OBSERVATIONS AND DATA PREPARATION

The WR nebula NGC 3199 around WR 18 was observed by the European Science Agency (ESA) X-ray telescope *XMM-Newton* on 2014 December 1 in revolution 2743 (Observation ID: 0744460101; PI: J.A. Toalá). The European Photon Imaging Camera (EPIC) was used in the Extended Full Frame Mode with the Medium Optical Filter. The total time of the observation was 56.8 ks with exposure times of 51.4, 53.4, and 53.2 ks for the EPIC-pn, EPIC-MOS1, and EPIC-MOS2, respectively.

We processed the EPIC observations using the *XMM-Newton* Science Analysis Software (SAS) Version 15.0 with the corresponding Calibration Access Layer obtained on 2016 February 26. The event files have been produced from the Observation Data Files by using the tasks *epproc* and *empproc* included in SAS. We identified periods of high-background level by creating light curves in the 10–12 keV energy range with a binning of 100 s for each of the EPIC cameras. We rejected times with count rates higher than 0.3 counts s^{-1} for the EPIC-pn camera and 0.2 counts s^{-1} for the MOS cameras. The resulting useful exposure times for the pn, MOS1, and MOS2 cameras are 36.1, 48.9, and 49.1 ks, respectively.

2.1. Spatial distribution of X-rays in NGC 3199

To study the spatial distribution of the X-ray-emitting gas in NGC 3199, we have used the *XMM-Newton* Extended Source Analysis Software package (XMM-ESAS) included in the current SAS version. We have followed the ESAS cookbook for the analysis of extended sources version 5.9² to create maps of the extended X-ray emission in NGC 3199 and to identify potential contaminant point sources.

We have created EPIC images in the energy bands 0.3–1.1, 1.1–2.5, and 2.5–5.0 keV that we label as soft, medium, and hard X-ray bands, respectively. Individual pn, MOS1, and MOS2 images were extracted, merged together, and corrected for exposure maps. Figure 2 shows the resultant background-subtracted EPIC image of the soft band and a color-composite picture of the three X-ray bands. Each X-ray image has been adaptively smoothed using the XMM-ESAS task *adapt* requiring 80, 80, and 30 counts for the smoothing kernel for the soft, medium, and hard band, respectively.

² <http://heasarc.gsfc.nasa.gov/docs/xmm/esas/cookbook/xmm-esas.html>

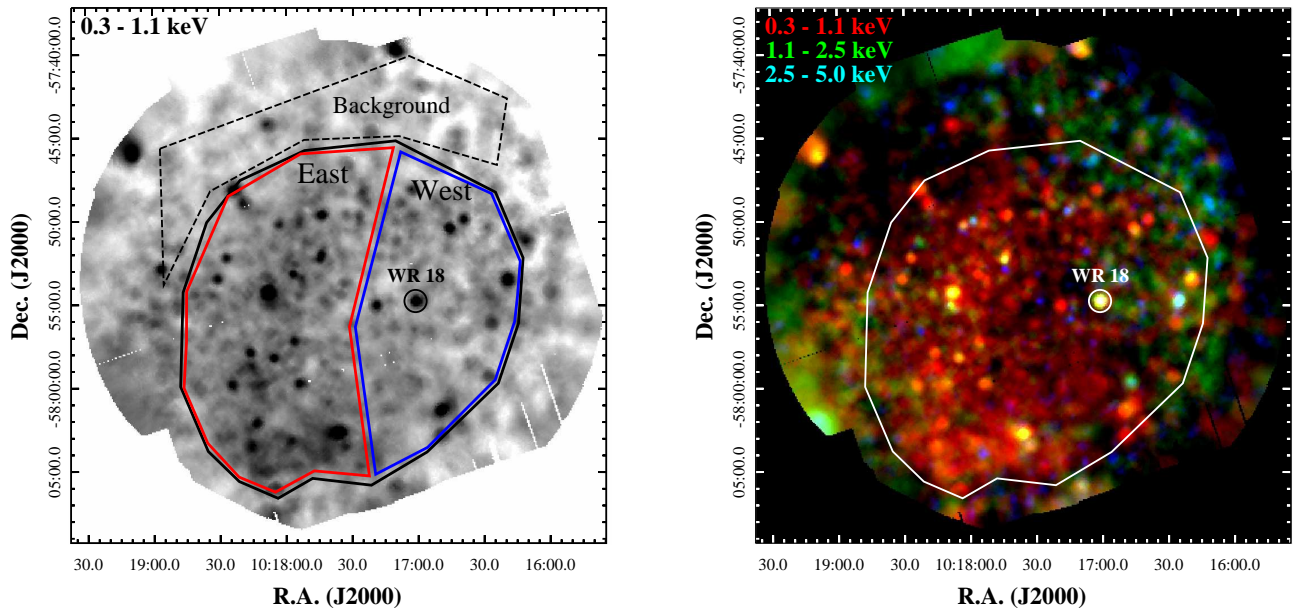


Figure 2. *XMM-Newton* EPIC (MOS1+MOS2+pn) exposure-corrected images of the X-ray emission from NGC 3199. Left: Soft band (0.3–1.1 keV). Right: Color-composite X-ray image. The colors red, green, and blue correspond to the soft, medium, and hard X-ray bands, respectively. The central star, WR 18, is shown with a circular aperture in both panels. The regions used for source spectral extraction are shown by solid lines whilst the background region by dashed line. No point sources have been excised from these images.

Figure 2 shows the presence of diffuse X-ray emission within the WR nebula NGC 3199, as well as a large number of point-like sources projected on the nebula. The central star, WR 18 is detected confirming the previous *Chandra* detection Skimmer et al. (2010). It seems that the most intense X-ray emission region is located toward the east of the nebula, in particular, the south-east region. Furthermore, the X-ray colors unveil spectral differences within the diffuse X-ray emission: the eastern regions emit predominantly soft emission (0.3–1.1 keV) while the western region emits significantly in the medium X-ray band (1.1–2.5 keV). To further illustrate this, we have used the CIAO *dmfilth* routine (version 4.8, Fruscione et al. 2006) to cut out all detected point-like sources and create a direct comparison between the nebular emission and the distribution of the X-ray-emitting gas. The identification of the point sources has been performed following the EPIC source finding thread³. This allowed us to perform a search for point sources in different energy bands (0.3–0.5 keV, 0.5–1.0 keV, 1.0–2.0 keV, 2.0–4.5 keV, and 4.5–12.0 keV) for the three EPIC cameras.

Figure 3 shows the comparison of the nebular [S II] and [O III] narrow-band images (in red and green, respec-

tively) presented in Fig. 1 with the resultant soft X-ray image (blue). It can be seen that the diffuse X-ray emission in NGC 3199 is delimited by the [O III] as in other WR nebulae, filling the cavities observed in narrow-band nebular line images. Moreover, the extended X-ray emission is considerably brighter toward the east.

2.2. Spectral extraction

To study the physical properties of the X-ray-emitting gas in NGC 3199, we have extracted different spectra: i) a spectrum that includes the extension of the main cavity as seen by the [O III] narrow-band emission, in order to estimate global properties of the diffuse X-ray emission, ii) spectra from smaller apertures to study variations in physical properties of the hot gas in the nebula, and iii) a spectrum of the central star WR 18. Three different polygonal apertures have been defined as shown in Fig. 2. We label the different spectra as NGC 3199, West, East, and WR 18.

All identified point-like sources have been removed prior to the spectral extraction. We only used the EPIC-pn spectra of the diffuse X-ray emission given the superior quality as compared to the EPIC-MOS spectra. In the case of the central star, however, the small numbers of counts forced us to use the three EPIC spectra for a better determination of the physical parameters (see below).

³ See <http://www.cosmos.esa.int/web/xmm-newton/sas-thread-src-find-stepbystep>

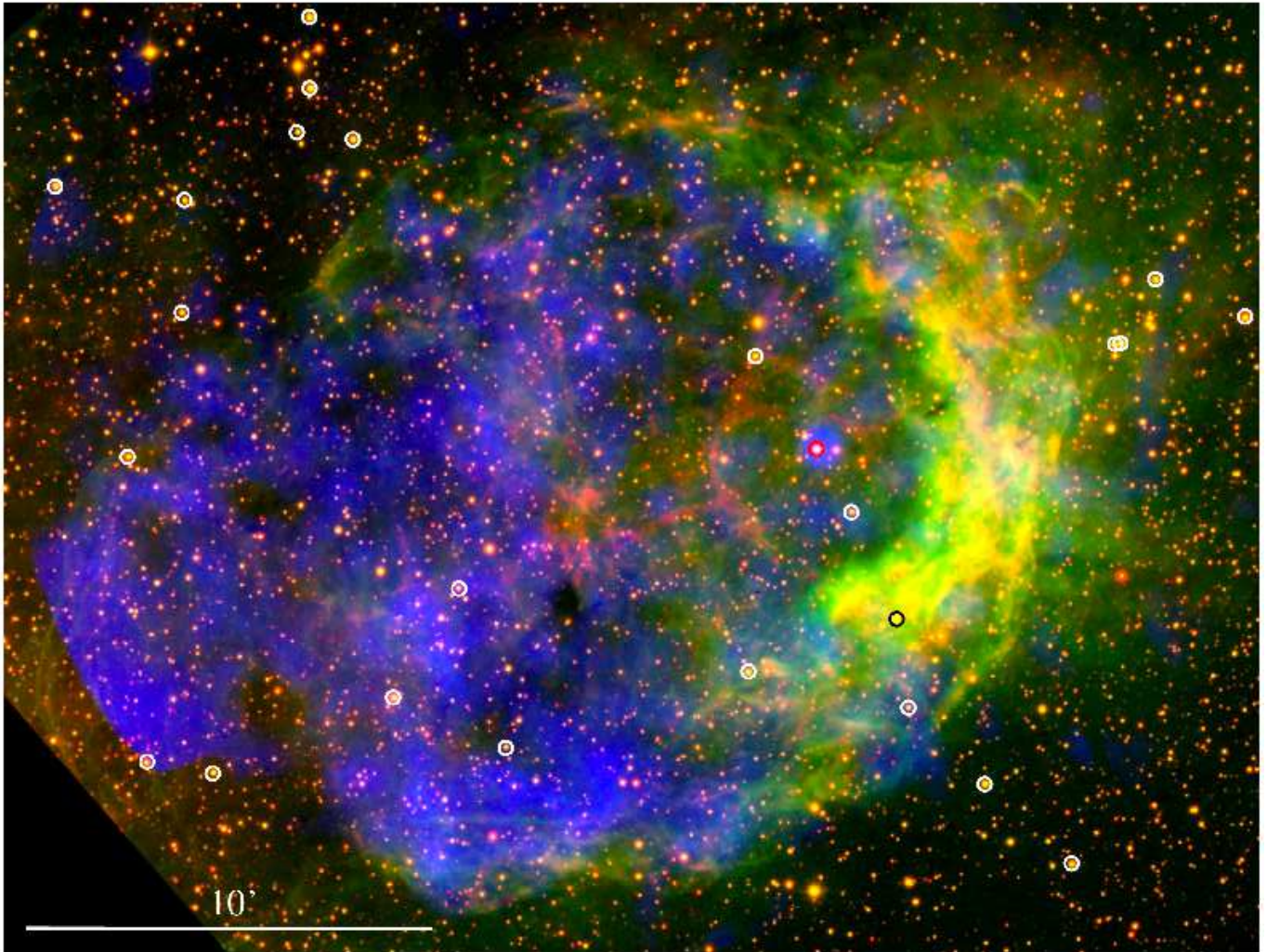


Figure 3. Color-composite image of NGC 3199 around WR 18. Red, green, and blue correspond to [S II], [O III], and the soft X-ray band (0.3–1.1 keV), respectively. All point-like sources have been cut out from the X-ray image except WR 18 (see text for details). The position of WR 18 is shown with a red circle whilst other circles mark the positions of the nearby Tycho-Gaia Astrometric Solution stars in the field of view. The black circle shows the position of the BOV star CD-57°3120 (see Discussion). North is up, east to the left.

Figure 4 presents all background-subtracted spectra.

WR nebulae are mainly located in the Galactic Plane, where the large absorption column density and significant background emission (e.g., Snowden et al. 1997) pose significant difficulties for the study of their extended X-ray emission. The spectrum of the background extracted from the region near the camera edges outside of NGC 3199, as defined in Fig. 2-left, has a significant contribution in the 0.3–3.0 keV energy range (Figure 5), where the diffuse X-ray emission from NGC 3199 mainly concentrates. Toalá et al. (2012) discussed the possibility of using EPIC Blank Sky observations (Carter & Read 2007) for the case of S 308. By definition, these blank fields have flat spectra, but they

do not adequately model the local Galactic background. While useful for the extraction of spectra of extragalactic objects, the Blank Sky observations can not be used for objects placed in the Galactic Plane (see also figure 3 and section 4.1 in Toalá et al. 2014). Therefore, the background spectrum extracted from the region surrounding NGC 3199 has been used.

3. RESULTS

All spectra have been modelled using XSPEC v.12.9.0 (Arnaud 1996) with a two-temperature *vappec* plasma emission model using a *tbabs* absorption model (Wilms et al. 2000). The resultant model spectra were compared with the observed spectra in the 0.3–3.0 keV

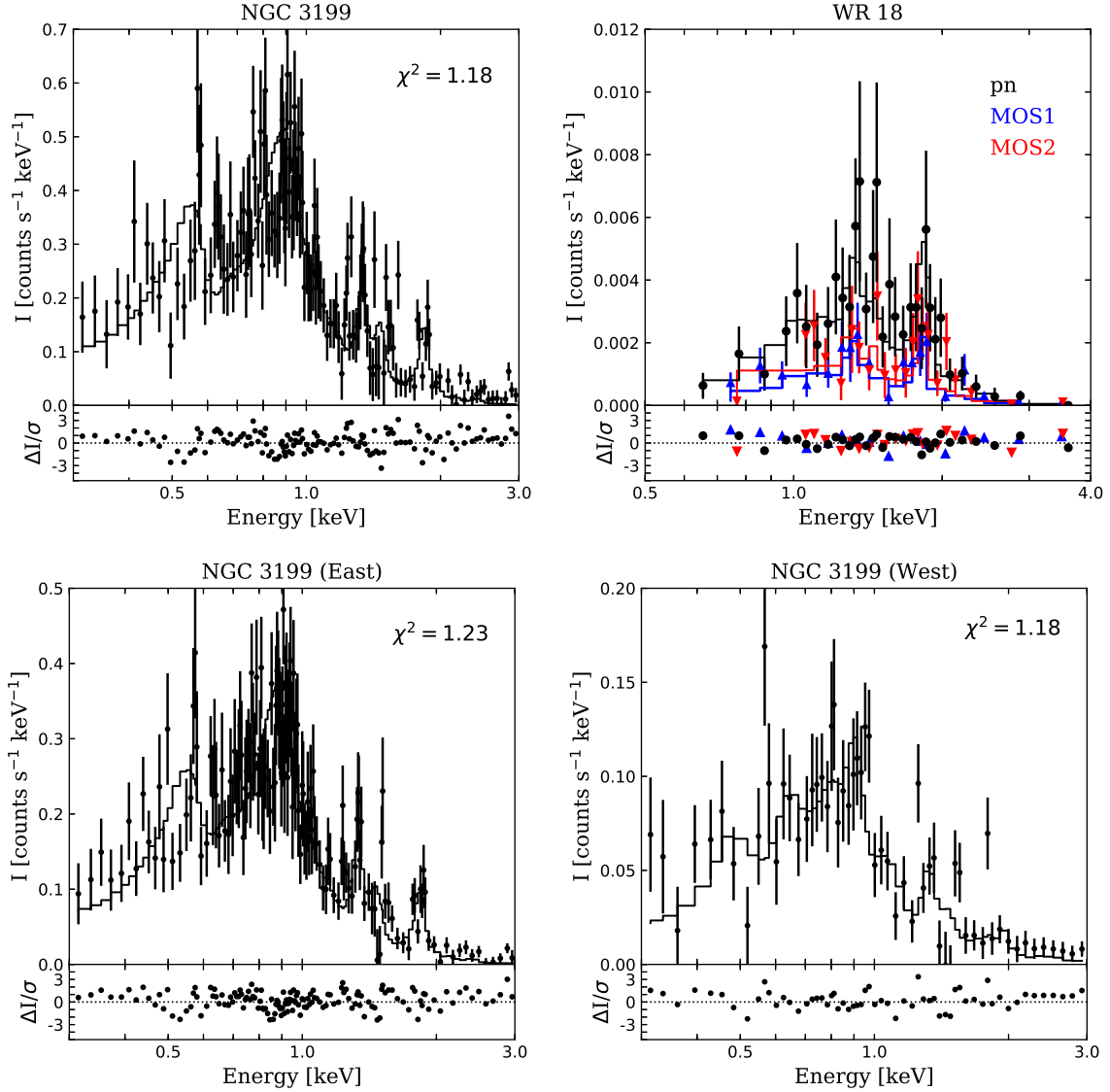


Figure 4. Background-subtracted spectra of the X-ray emission from NGC 3199. Top-left panel: Diffuse X-ray emission within NGC 3199. Top-right: EPIC spectra of WR 18. Bottom panels present the EPIC-pn spectra of the west and east regions as defined in Figure 2. The diffuse X-ray spectra (NGC 3199, East, and West) have been binned to 200 counts per bin for presentation. The best-fits to the data are shown with solid lines.

Table 1. Abundance estimates of NGC 3199

Element	X_{\odot} (Anders & Grevesse 1989)	X/X_{\odot} - WN star (van der Hucht et al. 1986)	X/X_{\odot} - NGC 3199 (Stock et al. 2011)	East	West
He	9.77×10^{-2}	9.52	0.91	0.91	0.91
C	3.63×10^{-4}	0.33	—	1.00	1.00
N	1.12×10^{-4}	52	0.52	0.52	$5.00^{+10.30}_{-3.20}$
O	8.51×10^{-4}	0.32	0.53	0.53	0.53
Ne	1.23×10^{-4}	4.96	1.38	1.38	1.38
Mg	3.80×10^{-5}	5.36	—	$4.01^{+0.87}_{-0.78}$	$4.37^{+2.67}_{-2.46}$
Si	3.55×10^{-5}	5.66	—	$3.20^{+0.83}_{-0.73}$	$3.40^{+5.60}_{-2.73}$
S	1.62×10^{-5}	2.93	1.20	1.20	1.20

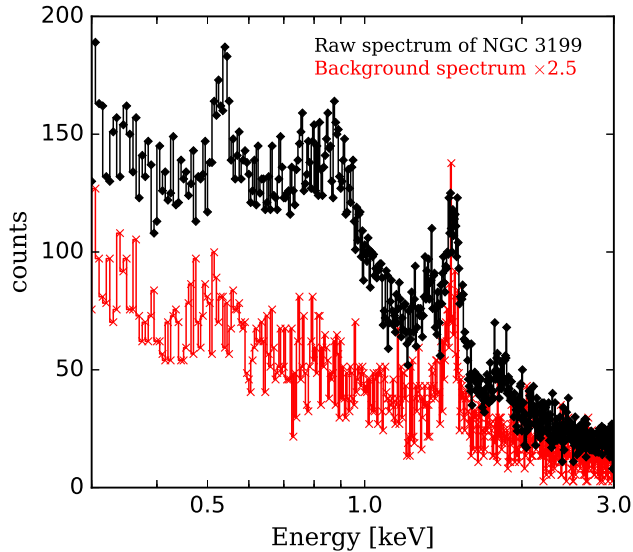


Figure 5. Background-unsubtracted raw EPIC-pn spectrum of NGC 3199 (black) and scaled EPIC-pn background spectrum (red). The prominent line at 1.5 keV in both spectra is the Al-K instrumental line.

energy range. We requested a minimum of 50 counts per bin for the spectral fit.

3.1. Global properties of the diffuse X-ray emission in NGC 3199

Figure 4-top left panel shows the background-subtracted EPIC-pn spectrum of the extended X-ray emission in NGC 3199. The spectrum is soft with emission mainly below 3.0 keV. The peak emission comes from energies around 0.7–1.0 keV which can be due to the Fe-complex and/or Ne IX lines. A secondary narrow peak is detected for energies below 0.6 keV which may correspond to the 0.58 keV O VII triplet. Other lines such as those coming from the He-like Mg XI at 1.36 keV and the Si XIII at 1.86 keV can also be identified. The diffuse X-ray emission count rate is 340 ± 10 counts ks^{-1} ($\approx 12,200 \pm 300$ counts) in the 0.3–3.0 keV energy range.

Following the analysis carried out for the X-ray emission in other WR nebulae, we modelled the diffuse X-ray emission in NGC 3199 using nebular abundances. As a first attempt we used the abundances reported by Stock et al. (2011, see Table 1) and a fixed absorption column density of $N_{\text{H}} = 5.35 \times 10^{21} \text{ cm}^{-2}$ (consistent with the averaged optical extinction $A_{\text{v}} = 2.92$; van der Hucht 2001). Other elements not reported by Stock et al. (2011), such as C, Mg, and Si, were initially fixed to their solar values (Anders & Grevesse 1989).

The first model resulted in a statistically good fit ($\chi^2 = 1.24$) with temperatures of $kT_1 = 0.18$ keV and

$kT_2 = 4$ keV, but the model was not able to fit the emission lines adequately. Better fits to the data were achieved by letting the Mg and Si abundances vary as free parameters. The best-fit model ($\chi^2 = 1.18$) has plasma temperatures of $kT_1 = 0.10_{-0.03}^{+0.01}$ keV ($T_1 \approx 1.2 \times 10^6$ K) and $kT_2 = 0.72_{-0.03}^{+0.04}$ keV ($T_2 \approx 8.5 \times 10^6$ K) and abundances of Mg and Si 3.8 and 3.0 times their solar values. The normalization parameters⁴ of each component are $A_1 = 7.50 \times 10^{-2} \text{ cm}^{-5}$ and $A_2 = 8.95 \times 10^{-4} \text{ cm}^{-5}$. The absorbed and intrinsic fluxes are $f_{\text{X}} = (1.10 \pm 0.10) \times 10^{-12} \text{ erg s}^{-1} \text{ cm}^{-2}$ and $F_{\text{X}} = (4.40 \pm 0.40) \times 10^{-11} \text{ erg s}^{-1} \text{ cm}^{-2}$. We note that the contribution of the second plasma component to the total unabsorbed flux is $\sim 8\%$.

At a distance of 2.2 kpc and taking an averaged radius of $10'$, the estimated X-ray luminosity and electron density are $L_{\text{X}} = 2.6 \times 10^{34} \text{ erg s}^{-1}$ and $n_{\text{e}} = 0.3 \text{ cm}^{-3}$.

We also tried other fits with O abundance as a free parameter taking into account the evident presence of the 0.58 keV O VII triplet in the spectrum. Even though this line appears strong, the O abundance converged to a value close to that reported for nebular abundances by Stock et al. (2011), as listed in Table 1. Other fits allowing N and Ne to vary also converge to their nebular values. Thus, the N, O, and Ne were fixed to these values. We also tried models allowing the absorption column density to vary, but no significant differences were found. Furthermore, we note that another model was attempted using abundances of a WN star (van der Hucht et al. 1986), as listed in Table 1, but did not produce a good fit ($\chi^2 > 2$).

In order to assess if the presence of the Mg and Si emission lines is real, and not an artifact of an inadequate background subtraction (see section 4.1 and figure 5 in Toalá et al. 2012), we show in Figure 5 the background-included spectrum of NGC 3199 and the background spectrum extracted from the EPIC-pn data for regions defined in Fig. 2. Whilst both spectra clearly show the instrumental Al-K emission line at 1.5 keV, only the spectrum from NGC 3199 shows the excess at ~ 1.4 keV and ~ 1.8 keV corresponding to the Mg XI and Si XIII emission lines, respectively. Thus, we are confident that these emission lines correspond to Mg- and Si-enriched material.

Finally, we tried to evaluate the contribution of the background X-ray emission (unresolved stars, background galaxies, ...) projected onto NGC 3199 by including an additional thermal component with temperature of 1 keV (see Townsley et al. 2011). The results of this spectral fit indicate that this component has a small

⁴ The normalization parameters is defined in XSPEC as $A = 10^{-14} \int \frac{n_{\text{e}} n_{\text{H}} dV}{4\pi d^2}$, where n_{e} , n_{H} , d , and V are the electron and hydrogen densities, distance, and volume, respectively.

contribution but does not change dramatically the parameters of the best-fit two-temperature model described above. Its main effect is a reduction of flux of the second plasma component from $\sim 8\%$ to $\sim 5\%$ of the total flux.

3.2. Variations in the physical properties of the X-ray emission in NGC 3199

In order to study the existence of variations in the plasma properties in NGC 3199, we extracted spectra from two different regions. The background-subtracted spectra of the eastern and western regions as defined in Figure 2 are shown in the bottom panels of Figure 4. The count rates for the eastern and western regions are 260 ± 10 counts ks^{-1} and 90 ± 5 counts ks^{-1} , corresponding to detections of $9,100 \pm 300$ counts and $3,200 \pm 160$ counts, respectively. The spectrum extracted from the eastern region shows very similar features as that obtained for the global spectrum. This is consistent with the fact that most of the diffuse X-ray emission comes from this region and the global spectrum will be dominated by its properties. On the other hand, the spectrum of the western region only shows a hint of the emission lines beyond 1 keV.

Before proceeding to the spectral analysis of the eastern and western regions, we used the SciPy PYTHON Kolmogorov-Smirnov (KS) statistics tests to evaluate similarities between spectra. This routine returns two values, the KS statistics and its significance (p -value). These parameters test the null hypothesis that the two samples were drawn from the same distribution: small (close to zero) KS statistics or large p -value means that the null hypothesis can not be rejected. The KS statistics between the west and east spectra is 0.47 with a significance of 6.76×10^{-24} . Therefore, we can easily reject the null hypothesis expecting that the physical properties differ between the two regions.

The NGC 3199 East and West spectra were initially modelled using the nebular abundances reported by Stock et al. (2011) with a fixed absorption column density of $N_{\text{H}} = 5.35 \times 10^{21} \text{ cm}^{-2}$, but we set the abundances of N, Ne, Mg, and Si as free parameters to improve the fits.

The best-fit model of the eastern region resulted in a reduced $\chi^2 = 1.23$ with best-fit parameters consistent with those found for the global spectral fit. The main plasma components are $kT_{1,\text{EAST}} = 0.11^{+0.01}_{-0.02}$ keV ($T_{1,\text{EAST}} \approx 1.3 \times 10^6$ K) and $kT_{2,\text{EAST}} = 0.71^{+0.04}_{-0.09}$ keV ($T_{2,\text{EAST}} \approx 8.2 \times 10^6$ K) with Mg and Si abundances of 4.0 and 3.2 times their solar values whilst N and Ne converged to their nebular values. The unabsorbed flux in the 0.3–3.0 keV energy range is $F_{\text{X,EAST}} = (2.70 \pm 0.40) \times 10^{-11} \text{ erg s}^{-1} \text{ cm}^{-2}$.

In the case of the western region, the best-fit model resulted in a reduced $\chi^2 = 1.18$ with a main plasma tem-

perature of $kT_{1,\text{WEST}} = 0.20^{+0.04}_{-0.02}$ keV ($T_{1,\text{WEST}} \approx 2.3 \times 10^6$ K) and N, Mg, and Si abundances of 5.0, 4.4, and 3.4 times their solar values. Unfortunately, XSPEC had trouble fitting the second plasma component and pointed out at the presence of a very hot plasma temperature ($kT_{2,\text{WEST}} > 2$ keV) that contributes to less than 6% of the unabsorbed flux of the model. The unabsorbed flux is $F_{\text{X,WEST}} = (5.90 \pm 1.50) \times 10^{-12} \text{ erg s}^{-1} \text{ cm}^{-2}$.

It is interesting to note the differences between the two regions: the western region has an enhanced N abundance in a similar way as that defined for WN stars (see Column 1 in Table 1) with higher plasma temperature, whilst the eastern region has N abundance closer to that found for the optical nebula with lower plasma temperature. Nevertheless, both regions present relatively similar Mg and Si abundances, 3–4 times their solar values, being larger for the western region.

3.3. X-rays from WR 18

The central star of NGC 3199, WR 18, is detected by all three EPIC cameras. Figure 4-top right panel shows the EPIC-pn, EPIC-MOS 1, and EPIC-MOS 2 background-subtracted spectra of this WR star. X-ray emission from WR 18 is mainly detected in the 0.5–4.0 keV energy range with strong features around ~ 1.5 keV and $\lesssim 2$ keV (see also figure 5 in Skinner et al. 2010). The final count rates from the pn, MOS1, and MOS2 cameras in the 0.4–4.0 KeV range is 4.28, 1.78, and 2.0 counts ks^{-1} , respectively.

To give a good characterization of the physical parameters from WR 18, we fitted simultaneously the three EPIC spectra using a two-temperature *vapex* model as for the diffuse X-ray emission. We followed the analysis by Skinner et al. (2010) for the *Chandra* observations of WR 18 and used abundances as those defined for a WN-type star (see column 3 in Table 1; van der Hucht et al. 1986). The best-fit model ($\chi^2 = 0.87$) has an absorbing hydrogen column density of $N_{\text{H}} = (1.27^{+0.80}_{-0.30}) \times 10^{22} \text{ cm}^{-2}$ and plasma components with temperatures of $kT_1 = 0.52^{+0.23}_{-0.28}$ keV and $kT_2 = 1.9^{+0.8}_{-0.8}$ keV, respectively⁵. The corresponding absorbed (unabsorbed) flux is $3.5 (28.2) \times 10^{-14} \text{ erg cm}^{-2} \text{ s}^{-1}$, which corresponds to a luminosity of $1.6 \times 10^{32} \text{ erg s}^{-1}$.

We also investigated the light curves of WR 18 obtained from the three EPIC cameras. We did not find any variation in the flux from WR 18 in the 0.5–4.0 keV energy range with the current *XMM-Newton* observations. We also produced soft (0.5–1.2 keV) and hard (1.5–4.0 keV) light curves and found similar results.

⁵ Note that the extinction toward WR 18 is higher than that estimated for the diffuse X-ray emission. This is a known issue and it is accepted to be due to self-absorption in the stellar wind (see, e.g., Oskinova et al. 2012, for the case of WR 6).

4. DISCUSSION

The deep optical images of NGC 3199 presented here unveil in unprecedented detail its true extension. Although the optical nebula has stronger H α emission towards the west of WR 18 (the southwest arc), it is in a shell that almost completely surrounds the star. Figure 1 shows that the nebula has an approximate diameter of $\gtrsim 20'$, with WR 18 displaced $\sim 4.7'$ from the center toward the west. This is in sharp contrast to the $4.8'$ radius suggested by Stock & Barlow (2010) from the inspection of H α narrow-band images from the Southern H α Survey (Drew et al. 2005; Parker et al. 2005). At a distance of 2.2 kpc, the physical size of NGC 3199 is $\gtrsim 7$ pc in radius. Another new morphological feature is the presence of a radial fan of emission protruding from the main nebula toward the west, and the radial rays of emission can be traced backward to WR 18 (see Fig. 1 upper right panel). This feature most likely results from shadowing instabilities (e.g., Williams 1999; Arthur & Hoare 2006): the dense western arc fragments into dense clumps and the UV flux from WR 18 passes through gaps between clumps to produce the radial features.

To the south-east we find more extended X-ray emission which appears bounded by [O III] thin curved structures as in the other WR nebulae studied in X-rays (S 308, NGC 2359, and NGC 6888; Toalá et al. 2012, 2015a, 2016). Extended [O III] structures have been seen in a number of WR bubbles (Marston 1995; Gruendl et al. 2000). The accepted scenario of this is that the wind from the central star and the pressurised hot bubble are pushing through surrounding denser media, such as an ejecta shell from an earlier evolutionary stage (RSG or LBV) or the ISM. The hot gas fills preferentially regions of more rarified gas densities and [O III] emission arises along the edges.

The strongest optically-emitting part of NGC 3199, the southwest arc, is actually seen to be in a direction from the WR star that is almost completely orthogonal to the direction of the proper motion of the star. As noted by Marston (2001), it is therefore not possible to reconcile the nebular morphology with the bow shock scenario of formation proposed by Dyson & Ghanbari (1989) in which the star has a proper motion toward the south-west. Our deeper images clearly show a more enclosing structure than that expected for a bow shock, with WR 18 off-center within this extended bubble structure.

Around 25% of massive stars are believed to have been ejected from their parent clusters and are *runaway* stars (Blaauw 1961; Fujii & Portegies Zwart 2011; Gies 1987; Hoogerwerf et al. 2000). Indeed, a runaway scenario could well explain any bow shock forming in the direction of the motion of the star. In order to check whether WR 18 is a runaway star, we need to determine

if it has a motion that is distinct from its surroundings and possibly in the direction of the putative bow shock, the south-western arc of NGC 3199.

The proper motion of WR 18 noted in Marston (2001) was derived from *Hipparcos* measurements. More recently, *Gaia* measurements in the DR1 release have become available (Gaia Collaboration et al. 2016). The Tycho-Gaia Astrometric Solution dataset (TGAS) of the *Gaia* DR1 release provides improved proper motions. The results continue to be consistent with the *Hipparcos* results (a proper motion toward the north-west direction; see Fig. 1) but with much smaller error. The overall proper motion is $(\mu_\alpha, \mu_\delta)_{\text{Gaia}} = (-5.98 \pm 0.17 \text{ mas yr}^{-1}, 3.48 \pm 0.16 \text{ mas yr}^{-1})$.

Within a radius of $20'$ around WR 18 there are 93 TGAS stars. Typical errors quoted for the proper motion of these stars are 1.5 mas yr^{-1} in R.A. and 1.2 mas yr^{-1} in Dec. If we consider all stars within 2 times this error value from the proper motion of WR 18 we find a total of 44 TGAS stars, or half of all TGAS stars in the region. In other words, there is a significant grouping of stars in the part of the sky containing WR 18 that have similar proper motions, both in terms of size and direction. To help illustrate this, we show in Fig. 3 the position of the TAGS stars that lie in the vicinity of our nebular images in white circles.

We may conclude that the proper motion of WR 18 gives no indication it is moving at some abnormal, runaway velocity with respect to its surroundings. Indeed, the cluster Westerlund 2 is found $57'$ away to the east and has a proper motion of $(\mu_\alpha, \mu_\delta)_{\text{Gaia}} = (-6.77 \text{ mas yr}^{-1}, 4.84 \text{ mas yr}^{-1})$ with a total error of 0.24 mas yr^{-1} (Kharchenko et al. 2013). Thus, the simplest interpretation of the proper motion of WR 18 is that it is part of the bulk Galactic motion of stars in the spiral arm of the Galaxy that contains both WR 18 and Westerlund 2.

Herschel PACS images (Pilbratt et al. 2010; Poglitsch et al. 2010) of the region also show that there is a large shell around WR 18 with WR 18 towards the western edge (see Fig. 6) but not toward the direction of the proper motion reported by *Hipparcos* or *Gaia*. The overdensity of materials to the west of the star would then naturally be caused by a pile-up of materials as the wind from WR 18 sweeps material up against the western edge of this large shell. The NGC 3199 nebula exhibits a particularly warm region of dust in the *Herschel* 100/160 μm ratio image shown in Figure 6. This is most likely due to the dust in this part of the nebula that is heated by the strong UV flux from WR 18. Although the [O III] 88 micron emission line is on the edge of the PACS broadband 100 μm spectral bandpass, Whitehead et al. (1988) concluded that the main emission mechanism in this region is due

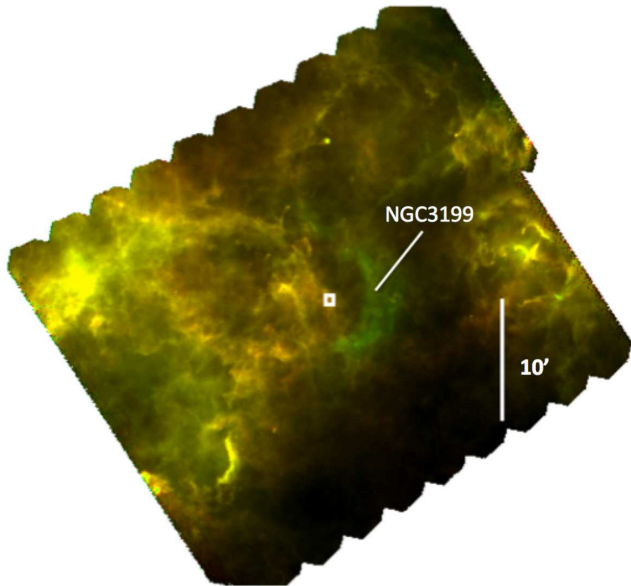


Figure 6. Two color *Herschel* PACS (Ob. ID 1342249269; PI: A. Marston) far infrared image at $100\ \mu\text{m}$ (green) and $160\ \mu\text{m}$ (red) wavelengths. The main nebula NGC 3199 exhibits an arc of high 100 to $160\ \mu\text{m}$ fluxes indicative of hot dust. The position of WR18 is shown by the white box at centre. North is up and east is to the left.

to radiative ionization from the central star and not by shocks (as it would be the case of a bow shock scenario).

To ensure that WR18 is the main source of ionization in NGC 3199, we searched for other OB stars in the vicinity of WR18. We took the 44 TGAS stars with similar proper motion as WR18 and searched for their spectral type. None of these stars have an O spectral type. We found only one BOV star (CD-57°3120) located $4.6'$ from WR18 (black circle in Fig. 3) projected on the bright $\text{H}\alpha$ arc. Nevertheless, WR18 will dominate the physics of NGC 3199. Its flux is almost 200 times larger than that estimated for CD-57°3120 (assuming standard stellar parameters for a B0V star from Cox 2000).

Our inescapable conclusion is that WR18 is not a runaway star and is likely to have been formed not far from its current position. The differences in spectral properties of the X-ray-emitting plasma and the reported variations in abundances are due to a combination of the initial inhomogeneous configuration of the ISM, which triggered different instabilities stirring the material unevenly, and the current metal-enriched fast stellar wind from WR18.

Optical emission-line studies of the chemistry of NGC 3199 have shown some apparent contradictory information between them. There appear to be some N-

enhanced ejecta-type of materials but there have also been reports of ISM abundances in NGC 3199. In our scenario it would be clear that most materials in the main part of the nebula should be associated with ISM materials that are from the giant shell inside of which exists WR18. But WR stars can typically have a clumpy ejecta phase, e.g. RSG or LBV phase. Ejected materials during a RSG or LBV phase is N-enriched (e.g., Stock & Barlow 2014). Clear evidence of metal-enriched materials is also seen close to WR18 (Marston 2001) and up to several parsecs away – which is a typical size for WR ring nebulae following an ejecta phase (e.g., Toalá & Arthur 2011).

WR stars exhibit highly-ionized species in their X-ray spectra, in particular those classified as WN stars (e.g., Skinner et al. 2010, 2012). Recently, Huenemoerder et al. (2015) presented the most detailed study of the X-ray spectrum from a WN4 type star, WR6. These authors used deep *Chandra*/HETGS observations to obtain a very high-resolution X-ray spectrum and reported the presence of a number of H-like and He-like emission lines, including strong lines of Mg XI at $1.36\ \text{keV}$ and Si XIII at $1.86\ \text{keV}$. Huenemoerder et al. (2015) concluded that the current wind of WR6 is ejected in a constant spherical expansion and that X-rays emerge from regions within 30 – 1000 stellar radii. If this would be also the case for WR18, it would help explain the high abundances of N, Mg, and Si in NGC 3199, specifically in the region around the star (e.g., the eastern region) and would imply that mixing with the ISM has been less efficient in that region.

Finally, it is interesting to speculate that the passage of a slowly expanding giant shell triggered the formation of the progenitor O star of WR18. An expansion rate of a few km s^{-1} is all that would be needed for the shell to advance to the current position of NGC 3199 in the million years or so that WR18 has taken to evolve to a WR star. WR18 would then be the result of a large clump that was triggered into star formation by a passing wave of material. There are numerous examples of triggered clumps of this kind in *Herschel* observations (Hill et al. 2011; Rivera-Ingraham et al. 2015; Zavagno et al. 2010).

5. SUMMARY AND CONCLUSIONS

The deep optical narrow-band images ($\text{H}\alpha$, $[\text{O III}]$, and $[\text{S II}]$) presented here, unveiled the true extension of the Wolf-Rayet nebula NGC 3199. The WR nebula around WR18 has an elongated shape with $18' \times 22'$ in size with its central star off-centered $4.7'$ toward the west. The analysis of the narrow-band images of NGC 3199 show a complex structure of radially-distributed filaments pointing outwards from WR18.

We presented the *XMM-Newton* discovery of the diffuse X-ray emission toward NGC 3199. These observations render NGC 3199 the fourth WR nebula detected

in X-rays. The current observations show that the diffuse X-ray emission is delimited by the [O III] narrow-band emission (as in the cases of S 308, NGC 2359, and NGC 6888 around WR6, WR7, and WR136) with a maximum toward the south-east region.

The global X-ray properties of NGC 3199 are similar to those found in other WR nebulae. The estimated intrinsic X-ray flux in the 0.3–3.0 keV energy band is $F_X = (4.40 \pm 0.40) \times 10^{-11} \text{ erg s}^{-1} \text{ cm}^{-2}$, which corresponds to a luminosity of $L_X = 2.6 \times 10^{34} \text{ erg s}^{-1}$ at a distance of 2.2 kpc. The dominant plasma temperature is $T \approx 1.2 \times 10^6 \text{ K}$ with a hotter component that contributes less than 8 per cent of the unabsorbed flux. The estimated electron density is $n_e = 0.3 \text{ cm}^{-3}$.

A careful analysis of the X-ray properties revealed temperature and abundances variations within the nebula: regions close to the main arc (the western region) are dominated by hotter gas with enhanced N, Mg, and Si abundances pointing to the current role of WR 18 in heating and enriching NGC 3199. The eastern region has lower plasma temperature with abundances similar to those reported previously for the nebular material implying that mixing is more important in this region. We suggest that these high abundances are due to the current metal-rich wind from WR 18 as detected in other WN4 stars (e.g., WR 6).

With the help of the *Gaia* first release and *Herschel* images we conclude that WR 18 is not a runaway star and it is more likely that the current shape of NGC 3199 is due to the initial inhomogeneous configuration of the ISM.

Finally, the properties derived from our *XMM-Newton* EPIC observations of WR 18 are in agreement to those reported previously based on *Chandra* observations. We further analyzed the X-ray light curves of WR 18 as obtained from the three EPIC cameras and we found no evidence of variations over timescales of the current observations ($< 50 \text{ ks}$).

ACKNOWLEDGEMENTS

We would like to thank the anonymous referee for helpful suggestions that improved the presentation of our results. This work was based on observations obtained with *XMM-Newton*, *Herschel*, and *Gaia* satellites. *XMM-Newton* is an ESA science missions with instruments and contribution directly funded by ESA Member States and NASA. *Herschel* is an ESA space observatory with science instruments provided by European-led Principal Investigator consortia and with important participation from NASA. The *Gaia* data have been processed by the *Gaia* Data Processing and Analysis Consortium (DPAC). Funding for the DPAC has been provided by national institutions, in particular the institutions participating in the *Gaia* Multilateral Agreement.

The authors thank Don Goldman (don@astrodon.com) for providing the narrow-band [S II], H α and [O III] images of NGC 3199. We thank G. Ramos-Larios for helping process the optical images. MAG acknowledges support from the grant AYA 2014-57280-P, co-funded with FEDER funds.

REFERENCES

- Anders, E., & Grevesse, N. 1989, *Geochim. Cosmochim. Acta*, 53, 197
- Arnaud, K. A. 1996, *Astronomical Data Analysis Software and Systems V*, 101, 17
- Arthur, S. J., & Hoare, M. G. 2006, *ApJS*, 165, 283
- Blaauw, A. 1961, *Bull. Astron. Inst. Netherlands*, 15, 265
- Carter, J. A., & Read, A. M. 2007, *A&A*, 464, 1155
- Chu, Y.-H., Guerrero, M. A., Gruendl, R. A., García-Segura, G., & Wendker, H. J. 2003, *ApJ*, 599, 1189
- Cox, A. N. 2000, *Allen's Astrophysical Quantities*, Fourth Edition
- Drew, J. E., Greimel, R., Irwin, M. J., et al. 2005, *MNRAS*, 362, 753
- Dwarkadas, V. V., & Rosenberg, D. L. 2013, *High Energy Density Physics*, 9, 226
- Dyson, J. E., & Ghanbari, J. 1989, *A&A*, 226, 270
- Dyson, J. E., & Williams, D. A. 1997, *The physics of the interstellar medium*. Edition: 2nd ed. Publisher: Bristol: Institute of Physics Publishing, 1997. Edited by J. E. Dyson and D. A. Williams. Series: The graduate series in astronomy. ISBN: 0750303069
- Esteban, C., Vilchez, J. M., Smith, L. J., & Clegg, R. E. S. 1992, *A&A*, 259, 629
- Fruscione, A., McDowell, J. C., Allen, G. E., et al. 2006, *Proc. SPIE*, 6270, 62701V
- Fujii, M. S., & Portegies Zwart, S. 2011, *Science*, 334, 1380
- Gaia Collaboration, Brown, A. G. A., Vallenari, A., et al. 2016, *A&A*, 595, A2
- Gies, D. R. 1987, *ApJS*, 64, 545
- Gosset, E., Nazé, Y., Claeskens, J.-F., et al. 2005, *A&A*, 429, 685
- Gruendl, R. A., Chu, Y.-H., Dunne, B. C., & Points, S. D. 2000, *AJ*, 120, 2670
- Hamann, W.-R., Gräfener, G., & Liermann, A. 2006, *A&A*, 457, 1015
- Hill, T., Motte, F., Didelon, P., et al. 2011, *A&A*, 533, A94
- Hoogerwerf, R., de Bruijne, J. H. J., & de Zeeuw, P. T. 2000, *ApJL*, 544, L133
- Huenemoerder, D. P., Gayley, K. G., Hamann, W.-R., et al. 2015, *ApJ*, 815, 29
- Kharchenko, N. V., Piskunov, A. E., Schilbach, E., Röser, S., & Scholz, R.-D. 2013, *A&A*, 558, A53
- Marston, A. P. 1995, *AJ*, 109, 1839
- Marston, A. P. 2001, *ApJ*, 563, 875
- Marston, A. P., & Meaburn, J. 1988, *MNRAS*, 235, 391
- Oskinova, L. M., Gayley, K. G., Hamann, W.-R., et al. 2012, *ApJL*, 747, L25
- Parker, Q. A., Phillipps, S., Pierce, M. J., et al. 2005, *MNRAS*, 362, 689
- Perryman, M. A. C., Lindegren, L., Kovalevsky, J., et al. 1997, *A&A*, 323
- Pilbratt, G. L., Riedinger, J. R., Passvogel, T., et al. 2010, *A&A*, 518, L1
- Poglitsch, A., Waelkens, C., Geis, N., et al. 2010, *A&A*, 518, L2
- Reyes-Pérez, J., Morisset, C., Peña, M., & Mesa-Delgado, A. 2015, *MNRAS*, 452, 1764

- Rivera-Ingraham, A., Marston, A., Martin, P., Ristorcelli, I., & Juvela, M. 2015, IAU General Assembly, 22, 2252224
- Skinner, S. L., Zhekov, S. A., Güdel, M., Schmutz, W., & Sokal, K. R. 2012, AJ, 143, 116
- Skinner, S. L., Zhekov, S. A., Güdel, M., Schmutz, W., & Sokal, K. R. 2010, AJ, 139, 825
- Snowden, S. L., Egger, R., Freyberg, M. J., et al. 1997, ApJ, 485, 125
- Stock, D. J., & Barlow, M. J. 2014, MNRAS, 441, 3065
- Stock, D. J., Barlow, M. J., & Wesson, R. 2011, MNRAS, 418, 2532
- Stock, D. J., & Barlow, M. J. 2010, MNRAS, 409, 1429
- Toalá, J. A., Guerrero, M. A., Chu, Y.-H., et al. 2016, MNRAS, 456, 4305
- Toalá, J. A., Guerrero, M. A., Chu, Y.-H., & Gruendl, R. A. 2015a, MNRAS, 446, 1083
- Toalá, J. A., & Arthur, S. J. 2011, ApJ, 737, 100
- Toalá, J. A., & Guerrero, M. A. 2013, A&A, 559, AA52
- Toalá, J. A., Guerrero, M. A., Gruendl, R. A., & Chu, Y.-H. 2014, AJ, 147, 30
- Toalá, J. A., Guerrero, M. A., Chu, Y.-H., et al. 2012, ApJ, 755, 77
- Townsley, L. K., Broos, P. S., Chu, Y.-H., et al. 2011, ApJS, 194, 15
- van der Hucht, K. A. 2001, New A Rev., 45, 135
- van der Hucht, K. A., Cassinelli, J. P., & Williams, P. M. 1986, A&A, 168, 111
- Whitehead, M. J., Meaburn, J., & Goudis, C. D. 1988, A&A, 196, 261
- Wilms, J., Allen, A., & McCray, R. 2000, ApJ, 542, 914
- Williams, R. J. R. 1999, MNRAS, 310, 789
- Zavagno, A., Anderson, L. D., Russeil, D., et al. 2010, A&A, 518, L101